THE ASTROPHYSICAL JOURNAL, 493:342–350, 1998 January 20

SIMILARITY SOLUTION FOR FORMATION OF A CIRCUMSTELLAR DISK THROUGH THE COLLAPSE OF A FLATTENED ROTATING CLOUD

KAZUYA SAIGO AND TOMOYUKI HANAWA
Department of Astrophysics, School of Science, Nagoya University, Chikusa-ku, Nagoya 464-01, Japan
Received 1996 December 30; accepted 1997 September 2

ABSTRACT

We present similarity solutions that describe the runaway collapse of a rotating isothermal disk and its subsequent inside-out collapse. The similarity solutions contain the sound speed c_s and the ratio ω of the specific angular momentum to the mass as model parameters. During the runaway collapse, the surface density of the disk is nearly constant in the central part and inversely proportional to the radius in the tail. As the central surface density increases by collapse, the central high surface density part shrinks its radius. Thus the surface density becomes a $1/r$ power law at the end of runaway collapse. In the subsequent inside-out collapse phase, the disk has two parts: an inner rotating disk in quasi-equilibrium and an outer dynamically infalling envelope. The inner disk and outer envelope are bounded by a shock wave. The mass and outer edge of the inner disk grow at a constant rate. The accretion rate is proportional to the cube of the sound speed, i.e., $\dot{M} \propto c_s^3/G$, where G denotes the gravitational constant. The similarity solution of the runaway collapse can reproduce numerical simulations of dynamical collapse of either rotating or magnetized disks. The similarity solution of the inside-out collapse denotes growth of a centrifugally supported circumstellar disk. This solution can apply to a protostar that accretes gas substantially through the disk.

Subject headings: accretion, accretion disks — circumstellar matter — hydrodynamics — stars: formation — stars: pre–main-sequence

1. INTRODUCTION

It is now widely accepted that nearly half of pre–main-sequence stars are associated with disks (see, e.g., Strom et al. 1989; Beckwith et al. 1990). Most of the disks are rotating and centrifugally supported at least in the central part. It is plausible that such a circumstellar disk is formed from a collapsing rotating cloud immediately after the formation of the protostar, i.e., the opaque core. In this paper we describe a model for the formation of a star and circumstellar disk from a collapsing rotating disk.

The formation of a star and circumstellar disk consists of two phases. The earlier phase is collapse of a cloud to form a dense opaque core, and the later phase is accretion onto the opaque core (see, e.g., Shu, Adams, & Lizano 1987). The earlier and later phases are often called the runaway and inside-out collapse, respectively. Circumstellar disk formation during the inside-out collapse has been studied extensively by Cassen & Moosman (1981), Terebey, Shu, & Cassen (1984), Boss (1989), Galli & Shu (1993a, 1993b), Stahler et al. (1994), and Li & Shu (1997). They computed the accretion of a rotating or magnetized gas onto the central opaque core with various methods. Cassen & Moosman (1981) and Stahler et al. (1994) computed the initial growth of circumstellar disks through the fall into the disk, neglecting the pressure force for simplicity. Terebey et al. (1984) and Galli & Shu (1993a, 1993b) included rotation and mean magnetic fields, respectively, as a perturbation in the model of Shu (1977). Li & Shu (1997) presented solutions for an isothermal magnetized disk. Although there is variety in the methods, the disk properties depend essentially on the initial condition, i.e., the density and velocity distributions at the onset of the inside-out collapse. When the accreting gas has a larger angular momentum, the formed circumstellar disk has a larger radius and a lower surface density.

The initial condition for the inside-out collapse is set during the collapse prior to the opaque core formation. Two types of collapse are considered for the formation of the opaque core. One is a quasi-static collapse, and the other is the dynamical one. The quasi-static collapse is driven by the ambipolar diffusion of the magnetic fields supporting the cloud (see, e.g., Lizano & Shu 1989; Basu & Mouschovias 1994; Li & Shu 1997), and dynamical collapse is initiated in a core exceeding the Jeans mass. It has not been observationally clear which type of collapse is common.

In this paper we consider the circumstellar disk formation following the dynamical collapse of a rotating disk. This is in part because the circumstellar disk formation following the quasi-static collapse has been studied extensively (Terebey et al. 1984; Galli & Shu 1993a, 1993b; Li & Shu 1997) and in part because the quasi-static contraction is theoretically less probable (Nakano 1997).

When an isothermal cloud collapses dynamically, the density profile approaches a power law $\rho \propto r^{-2}$, where ρ and r denote the density and the radius, respectively. It was first noticed by Larson (1969) and Penston (1969) for the collapse of a nonrotating and nonmagnetized spherical cloud (see Foster & Chevalier 1993 for more detail on the approach to the power law). It is also true for the collapse of a rotating cloud (Norman, Wilson, & Barton 1980; Narita, Hayashi, & Miyama 1984; Matsumoto, Hanawa, & Nakamura 1997), for that of a magnetized cloud (Scott & Black 1980; Nakamura, Hanawa, & Nakano 1995; Tomisaka 1996), and even for both (Basu & Mouschovias 1994) as far as the cloud is axisymmetric.

Larson (1969) and Penston (1969) found a similarity solution that accounts for the approach to the power law. Their similarity solution reproduces the numerical simulation of a collapsing gas sphere quantitatively up to the stage at which the central density reaches $\sim 10^{11}$ cm^{-3} and the central gas sphere becomes optically thick. After this stage, gas accretes onto the high-density opaque sphere. Hunter (1977) showed

that the similarity solution of Larson (1969) and Penston (1969) has a partner solution that describes the accretion onto the high-density opaque sphere. The similarity solution matches its partner at the stage at which the central sphere becomes opaque (see also Whitworth & Summers 1985).

A similarity solution for a collapsing rotating disk was first found by Narita et al. (1984). Recent numerical simulations (Nakamura et al. 1995; Tomisaka 1996; Matsumoto et al. 1997) have confirmed that the collapse of an isothermal rotating or magnetized cloud is well approximated by the similarity solution to the extent that the cloud is axisymmetric. Since their similarity solution is that of Larson (1969) and Penston (1969), it should have the partner that describes the inside-out collapse of a rotating disk and the formation of a circumstellar disk.

In this paper we describe the partner similarity solution for a collapsing rotating disk. According to numerical simulations, a dynamically contracting disk forms from a rotating cloud during its runaway collapse phase (Norman et al. 1980; Narita et al. 1984; Matsumoto et al. 1997). A dynamically contracting disk forms also from a magnetized cloud. When the disk forms from a parent cloud, the density at the center is from 10^2 to 10^3 times higher than the initial values. Once the disk has formed, the radial inflow within the disk dominates over the vertical accretion onto the disk. We neglect the vertical accretion and vertical structure of the disk for simplicity. Here we consider the disk evolution due to the radial inflow. We restrict ourselves to an axisymmetric disk for simplicity and search for similarity solutions.

Our solution shares common characteristics with the similarity solutions for a collapsing sphere obtained by Shu (1977) and Hunter (1977). (1) The density (or the surface density) and velocities are scaled by the sound speed. (2) The mass and the radius of the central high-density part decrease at a constant rate before the opaque core formation. (3) The mass accretion rate is constant and is proportional to the cube of the sound speed in the inside-out collapse phase.

Our similarity solution can apply to a magnetized disk if we replace the sound speed, c_s, and the gravitational constant, G, with the effective sound speed, $c_{s,\mathrm{eff}}$ (see, e.g., Shu, Adams, & Lizano 1987), and the effective gravitational constant, G_{eff} (see, e.g., Shu & Li 1997), respectively. The effective sound speed takes account of the magnetic pressure, and the effective gravitational constant take account of the magnetic tension. See Nakamura & Hanawa (1997) and references therein for more details on the application of our similarity solution to a magnetized disk.

In § 2 we describe the construction of our model equations, mathematical characteristics of our model equations, and methods of numerical computation. In § 3 our similarity solutions are presented. After the runaway and inside-out solutions are shown separately, we demonstrate an evolutionary model reproduced from the similarity solutions. This evolutionary model is arranged mainly for comparison with observations. In § 4 we compare our solutions with previously obtained similarity solutions, numerical simulations of collapses, and observations of disks.

2. SIMILARITY EQUATION

2.1. *Derivation*

We consider a geometrically thin disk consisting of an isothermal gas. For simplicity we assume that the disk is symmetric around the rotation axis. In cylindrical coordinates (r, φ), the hydrodynamical evolution of the disk is expressed as

$$\frac{\partial \Sigma}{\partial t} + \frac{1}{r}\frac{\partial}{\partial r}(r v_r \Sigma) = 0 , \tag{1}$$

$$\frac{\partial v_r}{\partial t} + v_r \frac{\partial v_r}{\partial r} - \frac{v_\varphi^2}{r} + \frac{c_s^2}{\Sigma}\frac{\partial \Sigma}{\partial r} - g_r = 0 , \tag{2}$$

and

$$\frac{\partial v_\varphi}{\partial t} + \frac{v_r}{r}\frac{\partial}{\partial r}(r v_\varphi) = 0 , \tag{3}$$

where Σ, $\boldsymbol{v} = (v_r, v_\varphi)$, g_r, and c_s denote the surface density, velocity, gravity, and sound speed, respectively. The gravity and surface density are linked by the Hankel transformation,

$$g_r(r, t) = -2\pi G \int_0^\infty k J_1(kr)\tilde{\Sigma}(k, t) dk , \tag{4}$$

and

$$\tilde{\Sigma}(k, t) = \int_0^\infty r J_0(kr)\Sigma(r, t) dr . \tag{5}$$

During the runaway collapse and the following inside-out collapse, the scale length varies; the disk shrinks before the formation of the central star, and expands apparently after the formation. The scale length is proportional to the time difference from the moment of the central star formation, $\propto |t - t_0|$. Around the moment of $t = t_0$ the appreciable changes in the density and velocity are restricted in the small central region. To "zoom up" the changes in the small central region, we introduce the zooming coordinates, which were originally developed by Bouquet et al. (1985) for a dynamically collapsing sphere. The transformation from the ordinary coordinates to the zooming coordinates is given by

$$x = \frac{r}{c_s(t - t_0)} , \tag{6}$$

$$s = \ln |t - t_0| , \tag{7}$$

$$\Sigma(r, t) = \frac{c_s}{2\pi G(t - t_0)}\sigma(x, s) , \tag{8}$$

$$v_r(r, t) = c_s \xi(x, s) , \tag{9}$$

$$v_\varphi(r, t) = c_s \zeta(x, s) , \tag{10}$$

and

$$g_r = \frac{c_s}{t - t_0}\gamma(x, s) . \tag{11}$$

Using this transformation, we rewrite equations (1)–(5) as

$$\frac{\partial \sigma}{\partial s} + \frac{1}{x}\frac{\partial}{\partial x}[x(\xi - x)\sigma] = -\sigma , \tag{12}$$

$$\frac{\partial}{\partial s}(\xi - x) + (\xi - x)\frac{\partial}{\partial x}(\xi - x) + \frac{1}{\sigma}\frac{\partial \sigma}{\partial x} - \frac{\zeta^2}{x} - \gamma = -(\xi - x) , \tag{13}$$

$$\frac{\partial}{\partial s}(x\zeta) + (\xi - x)\frac{\partial}{\partial x}(x\zeta) = -x\zeta\,, \tag{14}$$

$$\gamma(x, s) = \begin{cases} -\int_{-\infty}^{0} k\tilde{\sigma}(k, s)J_1(kx)dk & (x < 0)\,, \\ -\int_{0}^{+\infty} k\tilde{\sigma}(k, s)J_1(kx)dk & (x > 0)\,, \end{cases} \tag{15}$$

and

$$\tilde{\sigma}(k, s) = \begin{cases} \int_{-\infty}^{0} xJ_0(kx)\sigma(x, s)dx & (k < 0)\,, \\ \int_{0}^{+\infty} xJ_0(kx)\sigma(x, s)dx & (k > 0)\,. \end{cases} \tag{16}$$

For later convenience we define the disk mass as

$$\mu(x, s) = \int_0^x x'\sigma(x', s)dx'\,. \tag{17}$$

Integrating equation (12), we obtain

$$\frac{\partial \mu}{\partial s} + (\xi - x)\frac{\partial \mu}{\partial x} = -\mu\,. \tag{18}$$

Note that the term $\xi - x$ appears frequently in the above equations. It denotes the velocity in the zooming coordinates. The point fixed at a given r moves with the speed $-x$, in the zooming coordinates. This contribution is included in $\xi - x$.

When we assume the steady state ($\partial/\partial s = 0$), equations (12)–(16) reduce to the similarity equation of Narita et al. (1984). (Their eq. [2.9] contains an extra factor of 2 in the pressure force term. The extra factor is due to their inadequate thin-disk treatment. They evaluated the equation of motion on the mid-plane instead of integrating it over the height.) A steady solution in the zooming coordinates is a similarity solution in the ordinary coordinates. From the comparison of equations (14) and (18) we find that the similarity solution exists only when

$$\frac{x\zeta}{\mu} = \omega = \text{constant} \tag{19}$$

holds. The nondimensional parameter ω characterizes our solutions. Equation (19) means that the specific angular momentum, j, is proportional to the mass, M; $j(r) = \omega GM(r)/c_s$.

While equation (19) seems rather restrictive, it holds often in a disk formed by collapse of a rotating cloud. It holds when a disk has a constant surface density and rotates with a constant angular velocity. It holds more generally when the density and angular velocity are uniform. The density and angular velocity will be more or less uniform in a cloud before it is centrally condensed. During the collapse, the angular momentum distribution is conserved to the extent that the cloud is axisymmetric. If a disk forms from such a cloud, it has an angular momentum distribution denoted by equation (19). In fact, numerical simulations showed that equation (19) holds for a rotating collapsing disk formed by collapse of a rotating cloud (see, e.g., Matsumoto et al. 1997). Note that the disk mass is proportional to the time difference from the moment of the opaque core formation, $M \propto (t - t_0)$, for a given x. If equation (19) holds for a given range of M, it holds for a wider range of x when the time is closer to the epoch of the opaque core formation.

2.2. *Mathematical Characteristics*

Our similarity solutions have two singular points. One is the origin ($x = 0$), and the other is the sonic point ($\xi - x = -1$). The former is geometric and due to the polar coordinates. At the sonic point, the sound speed coincides with the gas velocity with respect to the zooming coordinates. We can show the latter singularity explicitly:

$$[(\xi - x)^2 - 1]\frac{\partial \sigma}{\partial x} + \sigma\left[\frac{(\xi - x)^2}{x} + \gamma + \frac{\omega^2\mu^2}{x^3}\right] = 0 \tag{20}$$

and

$$[(\xi - x)^2 - 1]\frac{\partial \xi}{\partial x} - (\xi - x)\left(\frac{1}{x} + \gamma + \frac{\omega^2\mu^2}{x^3}\right) = 0\,, \tag{21}$$

combining equations (12), (13), and (19) under the assumption of $\partial/\partial s = 0$. At the singular point, the velocity in zooming coordinates [$= c_s(\xi - x)$] coincides with the sound speed, and the phase velocity of a sound wave vanishes. Hydrodynamical equations for a steady state have a singular point at which the velocity is equal to the sound speed.

$$\frac{1}{x} + \gamma + \frac{\omega^2\mu^2}{x^3} = 0 \quad \text{at } \xi - x = \pm 1\,. \tag{22}$$

Equations (12)–(16) are regular at $x = \pm\infty$. Solutions have an asymptotic form of

$$\xi = \xi_\infty + O(x^{-2})\,, \tag{23}$$

$$\sigma = \frac{\lim_{x\to\infty}(x\sigma)}{x} + O(x^{-3})\,, \tag{24}$$

and

$$\mu = \left[\lim_{x\to\infty}(x\sigma)\right]x + O(x^{-1})\,. \tag{25}$$

Equations (12), (13), and (14) have singular equilibrium solutions,

$$\xi = 0\,, \tag{26}$$

$$\sigma = \frac{A_\pm}{x}\,, \tag{27}$$

$$\gamma = -\frac{A_\pm}{x}\,, \tag{28}$$

where

$$A_\pm = \frac{1 \pm \sqrt{1 - 4\omega^2}}{2\omega^2}\,. \tag{29}$$

When $\sigma < A_+/x$, the centrifugal force dominates over the gravity and thermal pressure. Accordingly, the disk expands to decrease σ. When $\sigma > A_-/x$, the thermal pressure dominates and accordingly the disk expands to decrease σ. When $A_-/x > \sigma > A_+/x$, the gravity dominates and the disk contracts to increase σ. Then the solution of $\sigma = A_+/x$ denotes a stable equilibrium solution, while that of $\sigma = A_-/x$ denotes an unstable one.

When $\omega = 0.5$, the two singular solutions degenerate. For $\omega > 0.5$ there is no singular equilibrium solution, since the gravity is weaker than the sum of the pressure and centrifugal forces for any density distribution.

2.3. *Numerical Procedures for $t < t_0$* Solutions

We obtained the numerical solution of equations (12)–(16) for $t < t_0$ (hence $x < 0$) iteratively. As a trial

surface density distribution we adopted

$$\sigma = \sum_{i=1}^{N} \frac{a_i}{\sqrt{x^2 + b_i^2}}, \tag{30}$$

where a_i and b_i are model parameters of this trial function. Substituting equation (30) into the Poisson equation and equation (1) we obtain

$$\gamma = -\sum_{i=1}^{N} \frac{a_i x}{b_i(b_i + \sqrt{x^2 + b_i^2})} \tag{31}$$

and

$$\mu = \sum_{i=1}^{N} \frac{a_i x^2}{b_i + \sqrt{x^2 + b_i^2}}. \tag{32}$$

Note that our trial function is regular at $x = -0$ and follows the asymptotic form (eqs. [23], [24], and [25]) in the limit $x \to -\infty$. The model parameters are adjusted to satisfy equation (20) when equations (30), (31), and (32) are substituted. Using this iteration, we found solutions for which the absolute value of the left-hand side of equation (20) is smaller than 5×10^{-5} $|\sigma|$ in the range $0.01 < -x < 100$. The value of N was set at 20 to achieve the accuracy.

When we substitute $N = 1$, $a_1 = -4$, and $b_1 = 2(1 - 4\omega^2)^{1/2}$, equations (30), (32), and (31) express the Narita et al. (1984) solution. The left-hand side of equation (20) is as much as $0.05\,|\sigma|$ around $x \simeq -7$ for their solution of $\omega = 0.3$.

To search for different solutions, we set the trial surface density distribution by defining $\tilde{\sigma}(k)$ by a spline function. Although the solutions obtained with the trial function $\tilde{\sigma}(k)$ have a larger (typically by a factor of 10) residual, they coincide with those obtained with the trial function given by equation (30), within the estimated errors. Our solutions are independent of the trial functions.

2.4. *Numerical Procedures for $t > t_0$ Solutions*

Solutions for the inside-out collapse ($t > t_0$) is much harder to obtain than that for the runaway collapse ($t < t_0$). As shown by Hunter (1977) and Whitworth & Summers (1985) for spherically symmetric collapse, the solutions for the runaway collapse phase should be connected continuously with the solutions for the inside-out collapse phase at $x = \pm\infty$ ($t = t_0$). In other words, there are two independent boundary conditions at $x = 0$ and $x = +\infty$, and there is no freedom for an auxiliary condition. Nevertheless, it should also be transonic except at $\omega = 0$. Near $x = 0$ the centrifugal force dominates over the gravity, and the flow should be quasi-static and therefore subsonic, $|\xi - x| \ll 1$. At $x = +\infty$ the flow is supersonic. The transonic point cannot be regular in principle, since the solution has no more freedom to satisfy equation (22). The transonic point must be discontinuous, and a shock wave must occur at the interface of supersonic and subsonic flows.

The self-similarity of the problem requires that the shock wave occupy a fixed position in the zooming coordinates, i.e., at $x = x_d$. Accordingly, the shock front moves outward at a velocity of $c_s x_d$ in the ordinary coordinates. Thus we apply the "isothermal" jump condition to the shock wave in the zooming coordinates. The conservation of mass and that of momentum are expressed as

$$\sigma_1(\xi_1 - x_d) = \sigma_2(\xi_2 - x_d) \tag{33}$$

and

$$\sigma_1[1 - (\xi_1 - x_d)^2] = \sigma_2[1 - (\xi_2 - x_d)^2], \tag{34}$$

respectively. Here the subscripts 1 and 2 indicate that the quantity is a preshock (upstream) or a postshock (downstream), respectively. When the surface density is discontinuous, it is very hard to obtain the integral of equations (15) and (16).

Instead of equations (15) and (16), we used

$$\gamma = -\mu x^{-2}, \tag{35}$$

in the computation of the gravity to obtain solutions for $t > t_0$. Equation (35) holds exactly for a spherical gas distribution and for a thin disk of $\sigma \propto x^{-1}$, but only approximately for an arbitrary disk. With equation (35) we can integrate equations (12) and (13) from $x = +\infty$ by the Runge-Kutta method. We also integrate them from $x = 0$ using the initial condition

$$\xi = \frac{A_+ - 2}{A_+(A_+ + \lambda)} \alpha x^{\lambda + 2}, \tag{36}$$

$$\eta = \frac{A_+}{x} + \alpha x^{\lambda}, \tag{37}$$

where

$$\lambda = \frac{-3 + \sqrt{4A_+ - 7}}{2}. \tag{38}$$

Equations (36) and (37) are asymptotic solutions in the limit of $x \to +0$ and denote the disk in quasi-static equilibrium. The parameter α denotes the amplitude of deviation from the stable equilibrium. The parameter α and positions of the shock wave were chosen so that the jump conditions can connect the two solutions.

3. SIMILARITY SOLUTION

3.1. *Solution in $t < t_0$*

Figure 1 shows the similarity solution in $t < t_0$, for $\omega = 0, 0.1, 0.2, 0.3, 0.4, 0.44, 0.48, 0.495$. The similarity solution exists only in the range $|\omega| < 0.5$. The ordinate denotes the nondimensional surface density σ, and the abscissa gives

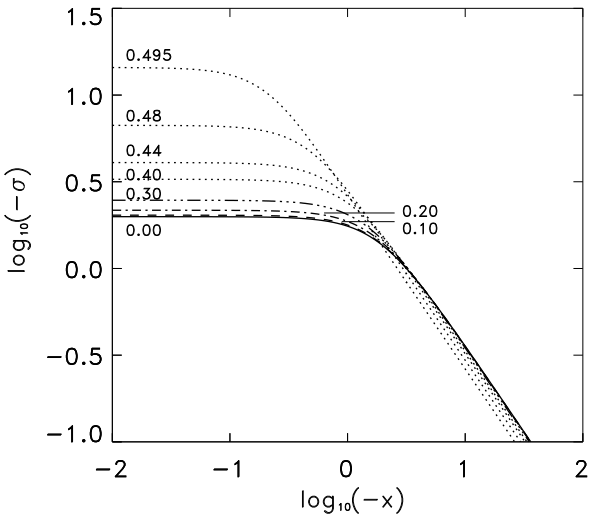

FIG. 1.—Similarity solution in the period $t < t_0$. The ordinate denotes the nondimensional surface density σ on a logarithmic scale, and the abscissa gives the nondimensional coordinates x. Each curve denotes a solution for a given ω, the value of which is indicated in the figure.

the nondimensional coordinate x, in the logarithmic scale. The surface density takes its maximum value at the origin for any ω, and the maximum value is higher for a higher ω. The surface density is nearly constant around the origin and is proportional to the inverse of the radius, $\sigma \propto x^{-1}$, in the tail of $|x| \gg 1$. The value of $x\sigma$ goes to an asymptotic value that is smaller for larger ω. Table 1 summarizes the central surface density and asymptotic value of $\lim_{x\to-\infty}(x\sigma)$ as a function of ω.

Figure 2 is the same as Figure 1, but for the infall velocity, $-\xi$. The radial velocity is proportional to the radial distance, $\xi \simeq x/2$, near the origin $0 \geq x \gg -1$. The radial velocity decreases to approach an asymptotic value, ξ_∞, as x decreases to $-\infty$. The asymptotic value, ξ_∞, is negatively larger for a smaller ω. Note that the infall velocity, $-\xi$, is smaller than 0.132 when $\omega = 0.495$. The similarity solution of $\omega = 0.495$ is close to the stable equilibrium solution. The value of $-\xi_\infty$ is 1.73 for $\omega = 0$ and appreciably larger than that obtained by Nakamura et al. (1995), 0.512. Computing the gravity correctly is necessary to estimate $-\xi_\infty$ appropriately.

The thin solid curve in Figure 2 denotes the sonic point, $\xi - x = 1$. Our solutions are smooth even when they pass the sonic point.

Figure 3 denotes the rotation velocity ζ. The rotation velocity is also proportional to the radius near the origin and nearly constant in the tail. The rotation velocity ζ is higher for a higher ω but lower than 1.44.

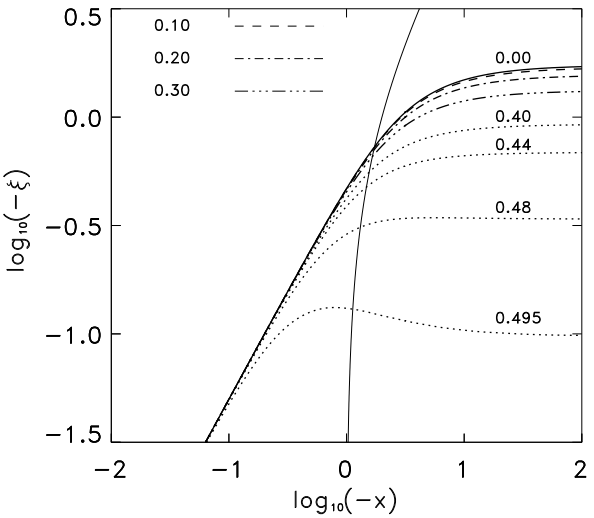

FIG. 2.—Same as Fig. 1, but for the nondimensional infall velocity ξ

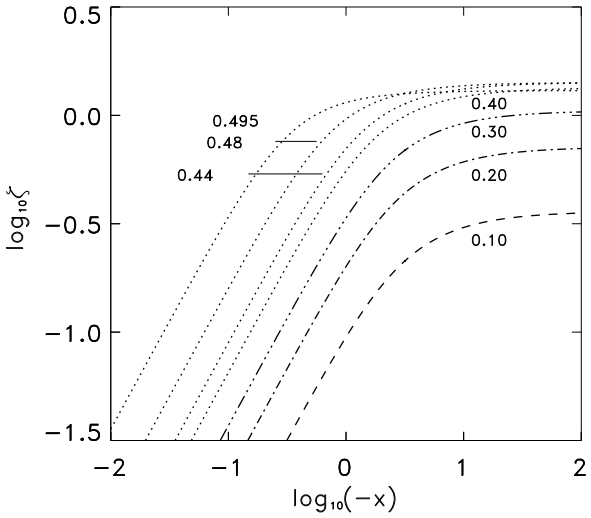

FIG. 3.—Same as Fig. 1, but for the nondimensional rotation velocity ζ

3.2. *Solution in $t > t_0$*

The solutions in $t > t_0$ denote the so-called inside-out phase (Shu et al. 1987) of the collapse. Figure 4 denotes the surface density as a function of the radius for $\omega = 0$, 0.1, 0.2, 0.3, 0.4, 0.44, 0.48, and 0.495. In the inside-out collapse phase $t > t_0$, the disk consists of two parts: the inner quasi-equilibrium disk and outer dynamically infalling flow. They are bounded by a shock wave, of which the radius is designated x_d. In the inner disk, $0 \leq x < x_d$, the surface density is well approximated by the stable equilibrium solution. The radius of the inner disk, x_d, is smaller for a smaller ω. The shock strength is larger for a smaller ω. When $\omega = 0$, the inner disk vanishes.

The infall velocity is shown in Figure 5 for the inside-out collapse phase $t > t_0$. The infall velocity is very small in the inner disk, while it is supersonic in the outer dynamically infalling flow. The infall velocity is negative (expanding) behind the shock wave ($x \leq x_d$). The dynamically infalling flow pushes the edge of the inner disk inward. The post-shocked gas expands gradually to restore the equilibrium. The infalling velocity has its maximum near the shock front. The maximum velocity is higher for smaller ω. When $\omega > 0.44$, the radial velocity is subsonic at any radius. Nevertheless the shock wave takes place, since the flow is supersonic with respect to the edge of the inner disk.

Figure 6 denotes the rotation velocity in the inside-out collapse phase $t > t_0$. The rotation velocity is almost constant both in the inner disk and in the outer region $x \lesssim 10$.

TABLE 1

CHARACTERISTIC VALUE OF SIMILARITY SOLUTIONS

	$t < t_0$				$t > t_0$	
ω	x_d	$\sigma_{x=-0}$	$\xi_{x=-\infty}$	$\lim_{x\to-\infty}(x\sigma)$	x_d	μ_d
0.0	−1.730	−1.989	−1.736	3.614	0.000	10.96
0.1	−1.724	−2.029	−1.695	3.604	0.107	10.60
0.2	−1.702	−2.166	−1.564	3.572	0.363	9.759
0.3	−1.657	−2.475	−1.326	3.504	0.676	8.512
0.4	−1.557	−3.268	−0.927	3.351	0.986	6.682
0.44	−1.476	−4.080	−0.687	3.224	1.091	5.651
0.48	−1.310	−6.688	−0.339	2.954	1.152	4.169
0.495.....	−1.130	−14.42	−0.098	2.631	1.110	3.057

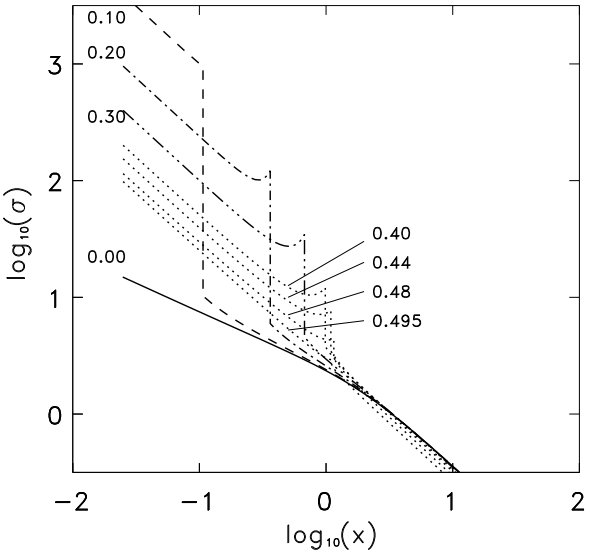

FIG. 4.—Similarity solution in the period $t > t_0$. The ordinate denotes the nondimensional surface density σ on the logarithmic scale, and the abscissa gives the nondimensional coordinates x. Each curve denotes a solution for given ω, the value of which is indicated in the figure.

In the middle region, $x_d < x \lesssim 5$, the rotation velocity is approximated by $\zeta \propto x^{-1}$. This rotation law means the specific angular momentum, j, is constant. In fact, the specific angular momentum is higher only by a factor of 1.2 at $x = 2x_d$ than at $x = x_d$ for $\omega = 0.3$.

3.3. *Disk Evolution in Ordinary Coordinates*

Substituting $c_s = 0.2$ km s^{-1} in the similarity solution of $\omega = 0.3$, we describe the dynamical collapse of a disk in the dimensional form. Figure 7 denotes the surface density evolution. The offset of the time is set as $t_0 = 0$ and the units of time are years. The abscissa denotes the radius in astronomical units on the logarithmic scale. The left ordinate denotes the surface density in units of molecules cm^{-2}, while the right ordinate denotes the equatorial density in units of molecules cm^{-3}. We assumed the mean molecular

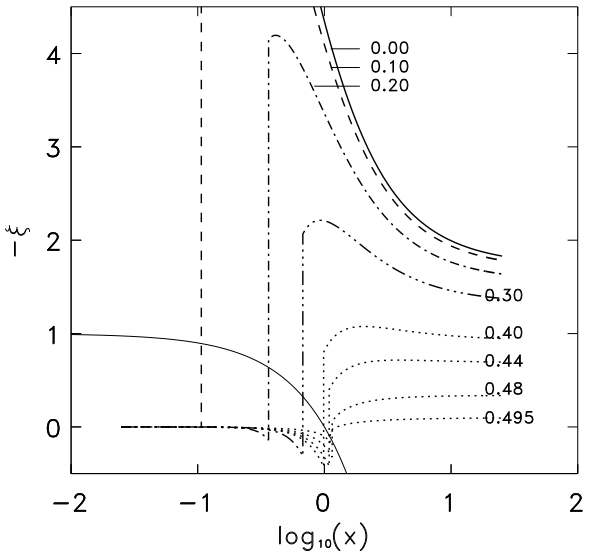

FIG. 5.—Same as Fig. 4, but for the nondimensional infall velocity ξ

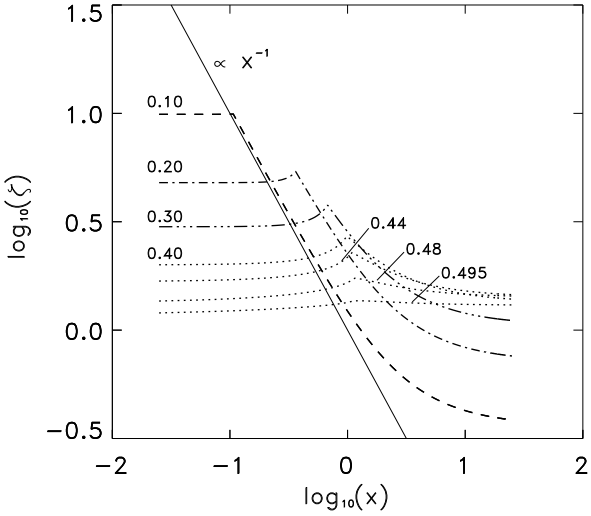

FIG. 6.—Same as Fig. 4, but for the nondimensional rotation velocity ζ

weight to be $\bar{m} = 2.3 m_{\rm H}$ to derive the surface and equatorial densities, where $m_{\rm H}$ denotes the mass of a hydrogen atom. The equatorial density is evaluated as

$$\rho_{\rm e} = \frac{\pi G \Sigma^2}{2 c_s^2}\,, \tag{39}$$

from the hydrostatic balance in the vertical direction. Each solid curve denotes both the surface and equatorial densities at a given epoch. Upper and lower dashed lines denote the stable and unstable equilibrium ($\sigma = A_{\pm}/x$), respectively.

The disk evolution is the transition from the initially uniform disk of a low surface density to the stable equilibrium of $\sigma = A_+/x$. At $t = 0$ yr, the surface density has a power-law distribution. In this sense, our solution is similar to the Larson-Penston solution and different from the solutions of Shu (1977). The latter denote the transition from a singular static gas sphere. Among them, Shu's expansion wave solution denotes the transition from the unstable singular equilibrium.

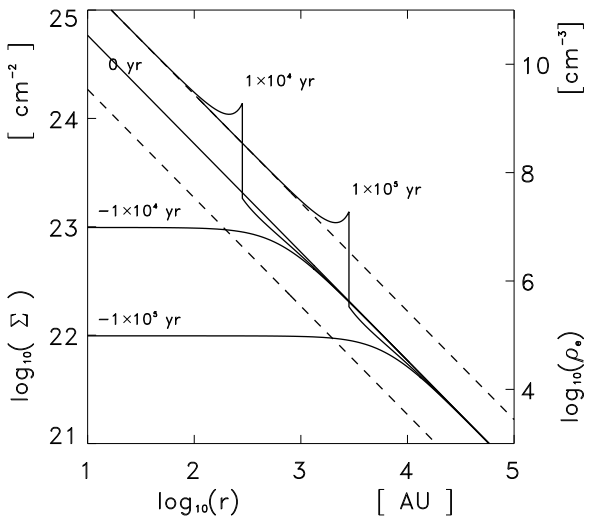

FIG. 7.—Surface density evolution for $\omega = 0.3$ and $c_s = 0.2$ km s^{-1}

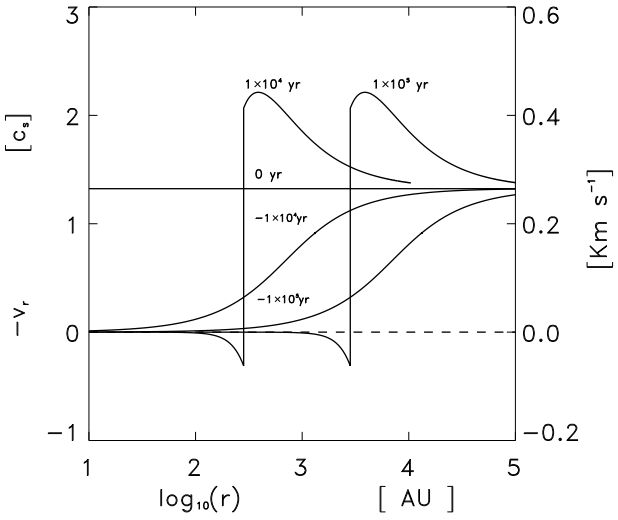

FIG. 8.—Same as Fig. 7, but for the radial velocity

In the early phase, $t < 0$ yr, the central disk becomes denser and smaller. In the late phase, $t > 0$ yr, the inner disk expands at a speed of $c_s x_d$. The mass of the inner disk increases in proportion to the time, $M_d = (c_s^3/G)\mu_d t$.

Figures 8 and 9 denote the evolution of radial and rotation velocities, respectively. The notation is the same as that of Figure 7, but for the ordinate. The ordinate denotes the infall velocity in the linear scale in Figure 8 and the rotation velocity in the logarithmic scale in Figure 9. In the outer dynamical flow the radial velocity dominates over the rotation velocity, while the latter dominates in the inner disk.

4. DISCUSSIONS

4.1. *Comparison with Other Similarity Solutions*

As shown in the previous section, our similarity solution for $t < t_0$ is similar to that of Narita et al. (1984); the surface density distributions differ only by 14%. Although the functional form of σ was an assumption in Narita et al. (1984), it has proved to be a good approximation to the smooth transonic solution. The sonic point selects a discrete solution in the sense that no regular solution is found in the close vicinity of it. Note that the regular transonic solutions exist continuously in the phase space for a collapsing sphere (Whitworth & Summers 1985), although the stable solutions are discrete (Ori & Piran 1988).

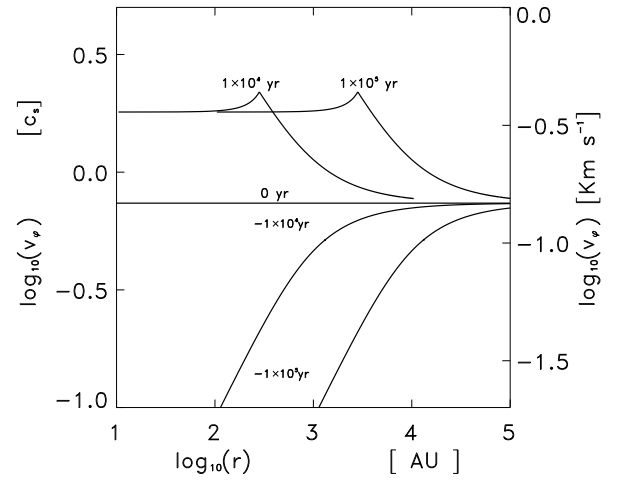

FIG. 9.—Same as Fig. 7, but for the rotation velocity

Our similarity solution for $t > t_0$ is similar to the solutions of Shu (1977), Hunter (1977), Terebey et al. (1984), and Galli & Shu (1993a, 1993b). All of them describe the inside-out collapse phase in which the central star or disk grows in mass and size. Both the solutions of Shu (1977) and those of Hunter (1977) are spherically symmetric although their initial conditions are different. Shu (1977) starts from a static gas sphere, while the solution of Hunter (1977) is continued from a dynamical collapse. Since our solution is continued from the dynamical collapse of a disk, it is closer to the Hunter (1977) solution.

The accretion rate is constant in the inside-out collapse phase in the similarity solutions of Shu (1977), Hunter (1977), and the present authors. The values are $0.975c_s^3/G$ for Shu, $46.9c_s^3/G$ for Larson-Penston (obtained by Hunter 1977), and 8.51 c_s^3/G for ours ($\omega = 0.3$). When the inside-out collapse starts from an unstable equilibrium, the accretion rate is $0.518c_s^3/G$ for $\omega = 0.3$. (Be careful not to take the accretion rate seriously, since the thin-disk approximation is not valid for unstable equilibrium.) It is smaller for a central star formed quasi-statically than for one formed dynamically. It is smaller for a dynamically collapsing disk than for a dynamically collapsing sphere.

The solutions of Terebey et al. (1984) and Galli & Shu (1993a, 1993b) denote disk formation during the inside-out collapse phase. Terebey et al. (1984) describes formation by rotation, while Galli & Shu (1993a, 1993b) do it by magnetic fields. Both start from a spherical gas distribution with no radial velocity at the onset of the inside-out collapse. Their solutions are constructed to reproduce the inside-out collapse of the core formed quasi-statically. Our solution is different from theirs, in that ours is continued from a dynamical collapse and the cloud already has a disk shape at the onset of inside-out collapse.

4.2. *Comparison with Numerical Simulations*

It has been well established in numerical simulations that the central density and angular velocity increase at an accelerated pace, $\rho_c \propto (t_0 - t)^{-2}$ and $\Omega_c \propto (t_0 - t)^{-1}$, during the isothermal collapse of a rotating cloud (cf. Norman et al. 1980; Narita et al. 1984). Our similarity solution explains these increases in ρ_c and Ω_c.

For more detailed comparison we choose Matsumoto et al. (1997) as an example of numerical simulations. They followed the collapse of a rotating cloud starting from fragmentation of a rotating filamentary cloud through formation of a disk. Although the disk collapse is roughly reproduced by a similarity solution, they found an appreciably large oscillation around the exact similarity. As the density increases owing to the collapse, the similarity solution becomes a better approximation. The similarity solution reproduces only the surface density well at first and also the radial velocity well later. Thus, we compared their average properties in a later phase with our similarity solution. Their simulation gives $\omega \simeq 0.3$, $\sigma_0 = -3.9$, $\lim_{x\to\infty}(x\sigma) = 6$, and $\xi_\infty = -1.6$. Our similarity solution gives a systematically smaller surface density.

Nakamura & Hanawa (1997) have shown that the similarity solution of $\omega = 0$ can be applied to the collapse of a magnetized disk if the sound speed and gravitational con-

stant are replaced by their effective values. The effective sound speed is expressed as

$$c_{s,\mathrm{eff}} = c_s \sqrt{1 + \alpha_s}\,, \tag{40}$$

and the effective gravitational constant as

$$G_{\mathrm{eff}} = G(1 - \alpha_s)\,, \tag{41}$$

where

$$\alpha_s = \left(\frac{B}{2\pi G^{1/2}\Sigma}\right)^2 . \tag{42}$$

The symbols B and α_s denote the magnetic flux density and the square of the mass per unit magnetic flux, respectively. The denominator on the right-hand side of equation (42) denotes the critical magnetic field for sustaining a disk for a given surface density σ. The magnetic field is weaker than the critical value for a dynamically contracting cloud (cf. Mestel 1965, 1966; Strittmatter 1966; Mouschovias & Spitzer 1976; Tomisaka, Ikeuchi, & Nakamura 1988). Substituting $\alpha_s = 0.1$, we obtain $\lim_{x\to\infty}(x\sigma) = 5.2$ and $\xi_{+\infty} \sim 2.5$ for model A of Tomisaka (1996) from his Figure 6. His numerical simulation gives a significantly higher surface density and infall velocity. Model A1 of Nakamura et al. (1995) has a stronger magnetic field and gives $\lim_{x\to\infty}(x\sigma) = 3.6$ with $\alpha_s = 0.2$. When the magnetic field is stronger, our similarity solution gives a better fit to a numerical simulation.

Both for rotating disks and for magnetized disks our similarity solutions give systematically smaller surface densities. This is mainly because the thin-disk approximation for gravity is not a quantitatively good approximation. The disk thickness is only a few times smaller than the radius. To assess the effects of the finite thickness, we compare the thin-disk solution with the two-dimensional solution for a rotating disk in equilibrium. Figure 10 denotes the surface density of a rotating disk in equilibrium as a function of ω. The thick curve denotes the exact two-dimensional solution obtained by Toomre (1982) and Hayashi, Narita, & Miyama (1982). The thin curve denotes our equilibrium solution, $\sigma = A_{\pm}/x$. The solid and dashed parts denote the stable and unstable branches, respectively. For $\omega = 0.3$ the thin-disk approximation underestimates the surface density by 10% and 65% for stable and unstable branches, respectively. The surface density of the dynamically contracting disk should lie between those of the stable and unstable equilibrium disks. Thus, our thin-disk approximation seems to underestimate the surface density by 30%–40%. This assessment is consistent with the above comparison with numerical simulations.

To obtain a better estimate for the accretion rate in the inside-out collapse phase, we integrated equation (12), (13), and (35), substituting the values of $\lim_{x\to-\infty}(x\sigma)$ and ξ_{∞} listed in Table 2. The obtained accretion rates are listed in the last column in the form of μ_d. The accretion rates are higher roughly in proportion to the assumed $\lim_{x\to\infty}(x\sigma)$ than those listed in Table 1.

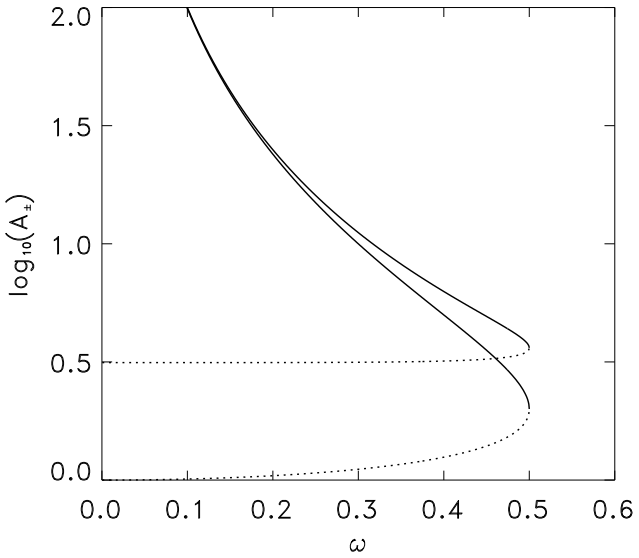

FIG. 10.—Comparison of thin-disk solutions with two-dimensional solutions for a rotating disk. The abscissa denotes the ratio of the specific angular momentum to the disk mass, $\omega = c_s\, j/GM$. The ordinate denotes the product of the surface density and the radius, $2\pi G\Sigma r/c_s^2$. The thick curve denotes the two-dimensional solution (Toomre 1982; Hayashi et al. 1982), and the thin curve denotes the thin-disk solution.

4.3. *Comparison with Observations*

Our similarity solution of $t < t_0$ is applicable to a dense core at a stage before the central star formation, and that of $t > t_0$ to a protostellar object. An example of a protostellar object of $t > t_0$ is L1551 IRS 5. The infall motion in L1551 IRS 5 is observed in the ^{13}CO (Ohashi et al. 1996) and $H^{13}CO^+$ (Saito et al. 1996) maps carried out with the Nobeyama Millimeter Array. The infall velocity is evaluated to be $\lesssim 0.8\ (\sin i)^{-1}$ km s^{-1} by Ohashi et al. (1996) and 0.6 km s^{-1} at 800 AU by Saito et al. (1996), where the symbol i denotes the inclination angle. The rotation velocity is 0.23 km s^{-1} at 900 AU. Our model is consistent with these infall and rotation velocities if we adopt $c_s = 0.2$ km s^{-1}. The accretion rate is evaluated to be (1.3–2.6) $\times 10^{-5}$ $M_{\odot}$ yr^{-1} at 600 AU by Ohashi et al. (1996) and $\sim 1.1 \times 10^{-5} M_{\odot}$ yr^{-1} by Saito et al. (1996). This large accretion rate is also consistent with our model. Also, the ^{13}CO and $C^{18}O$ maps of IRAS 05368+2557 and IRAS 04368+2557 (Ohashi et al. 1997) are consistent with the model in which a disk infalls in the outer part.

Similar inflow is detected for HL Tau with the Nobeyama Millimeter Array in the ^{13}CO emission (Hayashi, Ohashi, &

TABLE 2

SURFACE DENSITY AND INFALL VELOCITY FROM NUMERICAL SIMULATIONS .

ω	α_s	σ_0	$\xi_{x=-\infty}$	$\lim_{x\to-\infty}(x\sigma)$	μ_d	Reference
0.3.....	0.0	−3.9	~ -1.6	6	18.0	Matsumoto et al. 1997
0.0.....	0.1	...	~ -2.5	5.2	21.1	Tomisaka 1995
0.0.....	0.2	−2.7	> -1.2	3.6	9.21	Nakamura et al. 1995

NOTE.—Surface density and infall velocity are given in zooming coordinates. The expected accretion rate in the inside-out collapse is also listed.

Miyama 1993). The inflow has a radial velocity of 1 km s^{-1} and a typical surface density of $\sim 4 \times 10^{-2}$ g cm^{-3} ($\simeq 10^{22}$ cm^{-2}) at $r = 1400$ AU. These values produce the accretion rate of $0.9 \times 10^{-5}\ M_\odot\ yr^{-1}$, which is consistent with our solution. There is also an indication that the molecular gas has a rotation velocity of 0.2 km s^{-1} at $r = 700$ AU. If the shock front is located at $r = 700$ AU, the age of HL Tau is evaluated to be

$$\tau = 2 \times 10^4 \left(\frac{c_s}{0.2 \text{ km s}^{-1}}\right)^{-1} \left(\frac{r}{700 \text{ AU}}\right) \left(\frac{x_d}{0.676}\right)^{-1} \text{yr} . \quad (43)$$

Although this age seems to be too young for a T Tauri star, HL Tau is exceptional as a T Tau star. It is embedded in the molecular cloud and observed as the reflection nebula in the optical wavelength (Stapelfeldt et al. 1995). The photospheric luminosity of HL Tau is evaluated to be greater than $3\ L_\odot$, and accordingly the age is estimated to be $\lesssim 10^5$ yr. There are two possibilities for our solution to be consistent with observations. One is that the parameter ω is as small as 0.15 and hence $x_d = 0.223$ and $\tau = 6 \times 10^4$ yr. The other is that HL Tau is very young ($\sim 10^4$ yr) as inferred from the dynamical age of the bipolar outflows. Monin, Pudritz, & Lazareff (1996) evaluated the dynamical age to be 9000 yr.

Before closing this subsection, we refer to the processes and effects that are important but not taken into account in our similarity solution. The first one is the effect of finite disk thickness on the gravity as noted in § 4.2. Other problems are effects of nonaxisymmetry and viscosity. As pointed out by Nakamura & Hanawa (1997), the similarity solution is unstable against nonaxisymmetric perturbation. The disk tends to evolve into a bar, which is expected to fragment to form multiple star systems. The inside-out collapse for a multiple star system is an open problem. Another important issue is the evolution of the inner disk during the inside-out collapse. The inner disk is likely to accrete onto the central star by gravitational torque due to nonaxisymmetric perturbation and/or by turbulent origin viscosity, neither of which is taken into account in the present work.

5. SUMMARY

We have presented similarity solutions that describe the runaway collapse of a rotating isothermal disk and its subsequent inside-out collapse. We summarize the results as follows:

1. In the similarity solution, the specific angular momentum is less than a critical value, $j < 0.5GM/c_s$.
2. In the inside-out collapse phase, the disk has two parts: an inner rotating disk in quasi-equilibrium and an outer dynamically contracting envelope. The inner disk and outer envelope are bounded by shock waves.
3. The mass and outer edge of the inner disk grow at a constant rate. The mass accretion rate is

$$\dot{M} = 1.6 \times 10^{-5} \left(\frac{c_s}{0.2 \text{ km s}^{-1}}\right)^3 M_\odot \text{ yr}^{-1} \quad (44)$$

for $j = 0.3GM/c_s$. It is 8 times as much as that for the Shu (1977) solution.

The authors thank S. Inutsuka, T. Matsumoto, F. Nakamura, K. Nakayama, and K. Tomisaka for valuable discussions. This work is financially supported in part by Grants-in-Aids for Scientific Research (0840327) by the Ministry of Education, Science, Sports, and Culture, Japan.

REFERENCES

Basu, S., & Mouschovias, T. Ch. 1994, ApJ, 432, 720
Beckwith, S. V. W., Sargent, A. I., Chini, R. S., & Güsten, R. 1990, AJ, 99, 924
Boss, A. P. 1989, ApJ, 345, 554
Bouquet, S., Feix, M. R., Fijalkow, E., & Munier, A. 1985, ApJ, 293, 494
Cassen, P., & Moosman, R. 1981, Icarus, 48, 353
Foster, P. N., & Chevalier, R. A. 1993, ApJ, 416, 303
Galli, D., & Shu, F. H. 1993a, ApJ, 417, 220
———. 1993b, ApJ, 417, 243
Hayashi, C., Narita, S., & Miyama, S. M. 1982, Prog. Theor. Phys., 68, 1949
Hayashi, M., Ohashi, N., & Miyama, S. M. 1993, ApJ, 418, L71
Hunter, C. 1977, ApJ, 218, 834
Larson, R. B. 1969, MNRAS, 145, 271
Li, Z.-Y., & Shu, F. H. 1997, ApJ, 475, 237
Lizano, S., & Shu, F. H. 1989, ApJ, 342, 834
Matsumoto, T., Hanawa, T., & Nakamura, F. 1997, ApJ, 478, 569
Mestel, L. 1965, QJRAS, 6, 265
———. 1966, MNRAS, 133, 265
Monin, J.-L., Pudritz R. E., & Lazareff, B. 1996, A&A, 305, 572
Mouschovias, T. Ch., & Spitzer, L. 1976, ApJ, 210, 326
Nakamura, F., & Hanawa, T. 1997, ApJ, 480, 701
Nakamura, F., Hanawa, T., & Nakano, T. 1995, ApJ, 444, 770
Nakano, T. 1997, ApJ, submitted
Narita, S., Hayashi, C., & Miyama, S. M. 1984, Prog. Theor. Phys., 72, 1118
Norman, M., L., Wilson, J., R., & Barton, R., T. 1980, ApJ, 239, 968
Ohashi, N., Hayashi, M., Ho, P. T. P., & Momose, M. 1997, ApJ, 475, 211
Ohashi, N., Hayashi, M., Ho, P. T. P., Momose, M., & Hirano, N. 1996, ApJ, 466, 957
Ori, A., & Piran, T. 1988, MNRAS, 234, 821
Penston, M. V. 1969, MNRAS, 144, 425
Saito, M., Kawabe, R., Kitamura, Y., & Sunada, K. 1996, ApJ, 473, 464
Scott, E. H., & Black, D. C. 1980, ApJ, 239, 166
Shu, F. H. 1977, ApJ, 214, 488
Shu, F. H., Adams, F. C., & Lizano, S. 1987, ARA&A, 25, 23
Shu, F. H., & Li, Z.-Y. 1997, ApJ, 475, 251
Stahler, S. W., Korycansky, D. G., Brothers, M. J., & Touma, J. 1994, ApJ, 431, 341
Stapelfeldt, K. R., et al. 1995, ApJ, 449, 888
Strittmatter, P. A. 1966, MNRAS, 132, 359
Strom, K. M., Strom, S. E., Edwards, S., Cabrit, S., & Skrutskie, M. F. 1989, AJ, 97, 1451
Terebey, S., Shu, F. H., & Cassen, P. 1984, ApJ, 286, 529
Tomisaka, K. 1995, ApJ, 438, 226
———. 1996, PASJ, 48, 701
Tomisaka, K., Ikeuchi, S., & Nakamura, T. 1988, ApJ, 335, 239
Toomre, A. 1982, ApJ, 259, 535
Whitworth, A., & Summers, D. 1985, MNRAS, 214, 1